Circular Cylinder in Uniform Translation. Part 2: Unsteady Flow," *J. Fluid Mech.*, 79 (2), 257 (1977).
Crowe, C. T., "Drag Coefficients of Inert, Burning or Evaporating Particles Accelerating in Gas Streams," Ph.D. Thesis, University of Michigan, Ann Arbor (1962).
Deffenbaugh, F. D., and F. J. Marshall, "Time Development of the Flow about an Impulsively Started Cylinder," *AIAA J.*, **14**, 908 (1976).
Delaney, N. K., and N. E. Sorensen, "Low-Speed Drag of Cylinders of Various Shapes," NACA Tech. Note 3038 (1959).
Draper, W. R., and H. Smith, *Applied Regression Analysis*, John Wiley & Sons, Inc., New York (1968).
Eiffel, G., "Recherches à la Tour Eiffel," Paris (1907).
Fail, R., J. A. Lawford, and R. C. W. Eyre, "Low-Speed Experiments on the Wake Characteristics of Flat Plates Normal to an Air Stream," Aeronaut. Res. Council (Gt. Brit.), R. and M. No. 3120 (1959).
Goin, K. L., and W. R. Lawrence, "Subsonic Drag of Spheres at Reynolds Numbers from 200 to 10,000," *AIAA J.*, **6**, 961 (1968).
Hoerner, S. F., *Fluid Dynamic Drag*, published by the author, New Jersey (1958).
Ingebo, R. D., "Drag Coefficient for Droplets and Solid Spheres in Clouds Accelerating in Air Streams," NACA Tech. Note 3762 (1956).
Isaacs, J. L., and G. Thodos, "The Free-Settling of Solid Cylindrical Particles in the Turbulent Regime," *Can. J. Chem. Eng.*, **45**, 150 (1967).
Kry, P. R., and R. List, "Aerodynamic Torques on Rotating Oblate Spheroids; Angular Motions of Freely Falling Spheroidal Hailstone Models," *Phys. Fluids*, **17** (6), 1087 and 1093 (1974).
Lai, R. S., "Drag on a Sphere Accelerating Rectilinearly in a Maxwell Fluid," *Int. J. Eng. Sci.*, **12**, 645 (1974).
Lewis, J. A., and W. H. Gauvin, "Motion of Particles Entrained in a Plasma Jet," *AIChE J.*, **19**, 982 (1973).
Lunnon, R. G., "The Resistance of Air to Falling Spheres," *Phil. Mag.*, **47**, 1973 (1924).
Lunnon, R. G., "Fluid Resistance to Moving Spheres," *Proc. Roy. Soc. (London)*, **118A**, 680 (1928).
Mager, A., "Sudden Acceleration of a Laminar Boundary Layer by a Moving Belt," *AIAA J.*, **7**, 2247 (1969).
Mavis, F. T., "Virtual Mass of Plates and Disks in Water," *Proc. ASCE*, **96** (HY 10), 1947 (1970).
Mockros, L. F., and R. V. S. Lai, "Validity of Stokes' Theory for Accelerating Spheres," *Proc. ASCE*, **95** (EM3), 629 (1969).
Nakaguchi, H., K. Hashimoto and S. Muto, "An Experimental Study on Aerodynamic Drag of Rectangular Cylinders," (in Japanese) *J. Japn. Soc. Aeronaut. Space Sci.*, **16**, 1 (1968).
Odar, F., and W. S. Hamilton, "Forces on a Sphere Accelerating in a Viscous Fluid," *J. Fluid Mech.*, **18**, 302 (1964).
Odar, F., "Verification of the Proposed Equation for Calculation of the Forces on a Sphere Accelerating in a Viscous Fluid," *J. Fluid Mech.*, **25**, 591 (1966).
Pasternak, I. S., and W. H. Gauvin, "Turbulent Convective Heat and Mass Transfer from Accelerating Particles," *AIChE J.*, **7**, 254 (1961).
Robertson, J. A., C. Y. Lin, G. S. Rutherford and M. D. Stine, "Turbulence Effects on Drag of Sharp-Edged Bodies," *Proc. ASCE*, **98** (HY7), 1187 (1972).
Roos, F. W., and W. W. Willmarth, "Some Experimental Results on Sphere and Disk Drag," *AIAA J.*, **9**, 285 (1971).
Rudinger, G., "Effective Drag Coefficient for Gas-Particle Flow in Shock Tubes," *Trans. ASME*, **92D**, 165 (1970).
Schuyler, F. L., "Comment on 'Drag Coefficient of Small Spherical Particles," *AIAA J.*, **7**, 573 (1969).
Selberg, B. P., and J. A. Nicholls, "Drag Coefficient of Small Spherical Particles," *AIAA J.*, **6**, No. 3, 401 (1968).
Torobin, L. B., and W. H. Gauvin, "Fundamental Aspects of Solids-Gas Flow," *Can. J. Chem. Eng.*, Part I, **37**, 129 (1959); Part II, id. **37**, 167 (1959); Part III, id., **37**, 224 (1959); Part IV, id., **38**, 142 (1960); Part V, id., **38**, 189 (1960); Part VI, id., **39**, 113 (1961).
Wang, C. C., "Deceleration and Turbulence Effects on Sphere Drag Coefficient," M. Eng. Thesis, McGill University, Montreal, Canada (1969).
Wieselsberger, C., "Further Studies on the Laws of Fluids and Air Drag," *Physik. Zeit.*, **23**, 219 (1922).
Yoshizawa, A., "On the Mechanism of the Movement of a Separation Point," *J. Phys. Soc. Japan*, **39** (2), 509 (1975).

Manuscript received January 15, 1979; revision received May 2, and accepted May 7, 1979.

Measurement and Scale-Up of Secondary Nucleation Kinetics for the Potash Alum-Water System

JOHN GARSIDE

and

SLOBODAN J. JANČIĆ

**Department of Chemical and Biochemical Engineering
University College London
Torrington Place
London WC1E 7JE U.K.**

Secondary nucleation kinetics for potash alum in draft-tube baffled crystallizers have been determined from steady state crystal size distributions measured down to about 5 μm. Differences in nucleation rates were found for crystallizers of similar geometry but different capacity. Models relating the frequency of crystal/propeller collisions to crystallizer geometry and operating parameters were compared. In general, these successfully accounted for the observed differences in nucleation rates.

SCOPE

Nucleation rates in continuous crystallizers can be measured using the mixed suspension mixed product removal (MSMPR) concept (Randolph and Larson 1971). However, when the crystal growth rate is size-dependent in the range of sizes into which secondary nuclei are produced, the nucleation rate cannot be unambiguously calculated from the crystal size distribution (CSD) unless the size-dependent growth rate is determined by independent measurements. The first objective of the work reported here is to combine growth rates that had been measured previ-

Correspondence concerning this paper should be addressed to J. Garside. S. J. Jančić is now with Delft University of Technology, Laboratory for Process Equipment, Delft, Netherlands.

0001-1541-79-2923-0948-$01.25.

ously for the size range 3-1500 μm (Garside and Jančić 1976) with experimental steady state CSDs, to estimate the secondary nucleation kinetics of potash alum in an MSMPR crystallizer.

In any crystallizer, the overall nucleation rate is determined by the interaction of the secondary nucleation characteristics of the material being crystallized with the hydrodynamics of the crystal suspension. Previous authors (e.g., Ottens and de Jong 1972, 1973 and Evans et al. 1974) developed equations relating the nucleation rate in crystal suspensions to operating parameters using the results of fundamental studies on secondary nucleation (Clontz and McCabe, 1971) as a guide to the mechanisms involved. The second objective of the present work is to apply such concepts to a draft-tube baffled (DTB) crystallizer configuration, and investigate whether, on the basis of such models, nucleation rates measured at one scale of operation can predict rates at other scales and under different conditions.

CONCLUSIONS AND SIGNIFICANCE

To estimate the size-dependent secondary nucleation rate, a highly accurate determination must be made of the population density distribution and the size-dependent growth rate at sizes into which the majority of secondary nuclei are produced (less than about 10 μm). Such accuracy is not achieved in this study. Total nucleation rates, B_{TOT}, are therefore determined from the population density distribution, using the relationship that the total nucleation rate is equal to the total number of crysals in the crystallizer divided by the residence time.

Values of B_{TOT} from three crystallizers of capacities 1.3, 5, and 30 litre were correlated with concentration driving force, stirrer speed, and magma density. For similar values of these variables, nucleation rates in the 30 litre vessel were some 20 times higher than in the smaller crystallizers.

Different models for secondary nucleation rates in agitated crystallizers can be written in the form

$$B_{TOT} = K_N f(G) N^b \mu_j \Delta c^m$$

where $f(G)$ is a function of crystallizer geometry and size. The form of $f(G)$, as well as the values of b and j, depends on the assumptions made in developing the model. The equations of Ottens and de Jong (1972, 1973), of Evans et al. (1974), and of Jančić (1976) were used to predict nucleation rates in the 5 and 30 litre vessels from measurements at the 1.3 litre scale. All gave reasonable results. Scale-up of nucleation kinetics appears to be possible using relatively simple hydrodynamic models to describe the average flow characteristics of the crystal suspension.

The derivation of nucleation and growth kinetics from steady state crystal size distributions (CSD) in continuous mixed suspension, mixed product removal (MSMPR) crystallizers is a well-established technique. Size-dependent crystal growth rates, particularly in the small size range, complicates the analysis of such CSDs. If size-dependent growth occurs in ranges into which secondary nuclei are produced, then neither the growth nor the nucleation rates will be unambiguously deduced from the steady state CSD.

Results from a number of studies have indicated that very small crystals (say, less than about 20 μm in size) grow very slowly (Randolph and Cise 1972, Bujac 1976, van't Land and Wienk 1976, Rusli 1978, Garside 1978). In a previous paper, we reported crystal growth kinetics for potash alum crystals over the size range 3-70 μm (Garside and Jančić 1976). Growth rates were measured in a small (250 ml) batch crystallizer, using a Coulter Counter to follow the changing size of seed crystals. On the basis of these measurements, and previously published results for the size range 500-1700 μm (Mullin and Garside 1967), overall growth kinetics of potash alum in a typical laboratory crystallizer were estimated. These overall rates are strongly size-dependent for sizes less than about 100 μm, but become almost independent of size for crystals larger than about 500 μm.

In this work, these independently-measured size-dependent growth rates are combined with experimental CSDs from continuous MSMPR crystallizers to obtain size-dependent secondary nucleation rates and so avoid having to make limiting assumptions concerning either the growth or nucleation rates of very small crystals (Youngquist and Randolph 1972, Randolph and Cise 1972).

Studies of secondary nucleation show that secondary nuclei are easily produced in size ranges between about 1 and 20 μm as a result of low energy contacts between a growing crystal and a solid rod (Garside and Larson 1978, Garside et al. 1979). The rate of nuclei production arising from collisions of crystals with the stirrer, crystallizer, or other crystals depends on the surface morphology of the crystals and on the collision energy and collision frequency (Clontz and McCabe 1971, Bauer et al. 1974, Larson and Bendig 1976). Energy and frequency factors are determined by the hydrodynamic characteristics of the crystallizer/crystal suspension system. Several flow models relating these factors to crystallizer parameters have been published (e.g. Ottens and de Jong 1972, 1973, Bennett et al. 1973, Evans et al. 1974). In the second part of this article, such models are used to examine the influence of scale on nucleation kinetics.

EXPERIMENTAL TECHNIQUES AND PROCEDURE

Full details of the crystallizer design and experimental procedure have been published previously (Jančić and Garside 1975; Jančić 1976). Three crystallizers of similar, but not identical, geometry are used. Working capacities are 1.3, 5, and 30 litre, and they are of the same design described by Jones

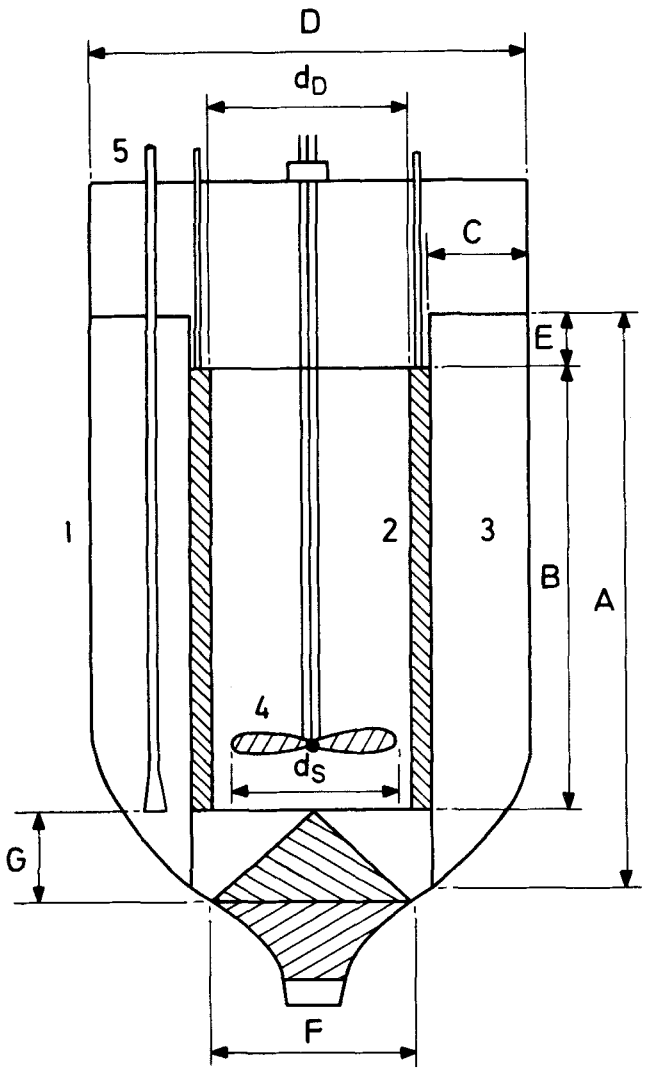

Figure 1. Crystallizer geometry (see Table 1 for dimensions of the three crystallizers).

TABLE 1. DETAILS OF CRYSTALLIZER GEOMETRY (DIMENSIONS DEFINED IN FIGURE 1)

Dimension	Working capacity 1.3 litre	5 litre	30 litre
A, (mm)	143	235	378
B, (mm)	110	175	300
C, (mm)	22	27	65
D, (mm)	110	170	300
E, (mm)	13	25	40
F, (mm)	43	84	140
G, (mm)	25	60	50
d_D, (mm)	45	83	136
d_s, (mm)	40	65	120
p, (−)	0.75	0.50	1.00
V_{prop}/V_C, (−)	6.41×10^{-3}	2.95×10^{-3}	6.92×10^{-3}

and Mullin (1973). Figure 1 shows a crystallizer, and the important dimensions are given in Table 1.

The crystallizers are cylindrical glass vessels, *1*, fitted with a hollow, stainless steel draft-tube, *2*, through which cooling water can be circulated. The draft-tube is supported in position by four vertical stainless steel baffles, *3*, positioned between the draft-tube and the vessel wall. Agitation is provided by a three-bladed marine type propeller, *4*, located on the center line of the draft-tube. Polyethylene propellers are used in the two smaller crystallizers, while that employed in the 30 L crystallizer is constructed of stainless steel. Subsequent experiments in which the stainless steel propeller is coated with polyethylene show no differences in the nucleation rate (Manjaly 1978) and so results from these three vessels can be compared on a realistic basis.

Feed solution was introduced in the draft-tube just above the propeller, which acted as an internal pump and directed the flow of suspension downward, thoroughly mixing the feed solution with the circulating magma. Product crystals are removed intermittently through a 5 mm i.d. glass tube, *5*, extending to the lower end of the draft-tube. Not more than 10% of the tank contents are extracted during a short period at regular intervals. The bottom end of the off-take tube is shaped into a cone, this geometry being found to favor isokinetic removal of samples that are representative of the crystallizer contents. Preliminary tests involving measurements of the transients undergone by a predetermined CSD when washed out of the crystallizer by saturated solution show that all three crystallizers conform to the mixed suspension, mixed product removal concept (Jančić 1976).

The potash alum/water system is used in the present study. All experiments are performed at 30°C, supersaturation being produced by cooling. Solution concentration in the crystallizer, and hence the operating supersaturation, is determined via solution density measurements. The pyknometric method used is estimated to give 95% confidence limits in the measured values of Δc equivalent to about ±30% at $\Delta c = 10^{-3}$ kg hydrate/kg solution and about ±4% at 10^{-2} kg hydrate/kg solution (Jančić, 1976).

The steady-state crystal size distribution is measured using both sieves and a multichannel Coulter Counter (Model TA). British Standards specification sieves (British Standards, 1969) are used to cover the size range between 37 and 1680 μm, while a 280 μm Coulter orifice tube enables measurements to be made in the range 5 to 112 μm.

Full details of the Coulter Counter technique have been given elsewhere (Jančić and Garside 1975; Jancic 1976), but two essential features of the method must be emphasized here. Firstly, the samples for Coulter Counter analysis are obtained from the crystallizer by withdrawing a 1 ml slurry sample with a pipette. This sample is then introduced directly into the Coulter Counter sampling beaker through a 125 μm aperture wiremesh. The small suspended crystals (<125 μm) are thus not subjected to filtration, washing, or drying steps which would likely affect the original size distribution. Second, the electrolyte solution used for the Coulter Counter analysis is a saturated potash alum solution at the crystallizer operating temperature, with the solution temperature thermostatically controlled. Changes in crystal size distribution resulting from crystal growth or dissolution in the sampling beaker are thus minimized.

DERIVATION OF THE NUCLEATION RATE

For an MSMPR crystallizer operating at steady state, the general population balance when the death of particles is assumed negligible reduces to (Randolph and Larson 1971)

$$\frac{d[n\,G(L)]}{dL} + \frac{n}{\tau} - B(L) = 0 \qquad (1)$$

where the first term represents the net rate of loss of crystals of size L to $L + dL$ by growth, the second term represents the rate of loss of crystals by flow out of the crystallizer, and the third term is the birth rate or rate of formation of new crystals. Equation (1) may be rewritten

$$\frac{1}{\tau}\int_0^\infty n\,dL = -\int_0^\infty d[n\,G(L)] + \int_0^\infty B(L)dL$$

and so

$$B_{TOT} = \frac{1}{\tau}\int_0^\infty n\,dL = n^0G^0 + B(L)_{TOT} \qquad (2)$$

since $n^\infty\,G^\infty$ is zero as $n^\infty \to 0$.

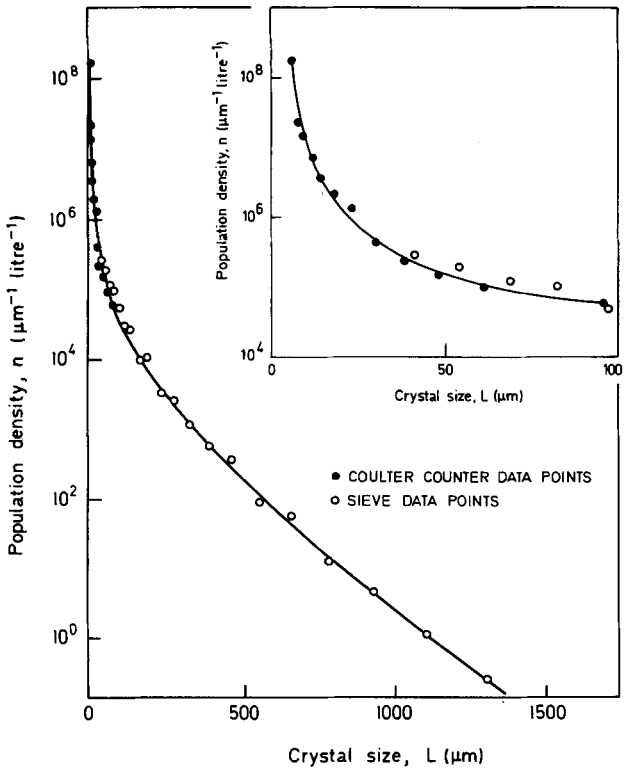

Figure 2. Population density plot for a typical run. Inset shows the small size range on an enlarged scale.

The first term in Equation (2) represents the total nucleation rate. Since on average all the crystals in the crystallizer are removed in one residence time, this is given by the total number of crystals in the crystallizer divided by the residence time. This total nucleation rate is made up of 1) a convective flux of nuclei across the boundary $L = 0$, i.e., the $n^0\,G^0$ term, and 2), the size-dependent secondary nucleation rate which produces particles at a rate $B(L)_{TOT}$ over a range of sizes.

The slope of a population density plot (i.e. the plot of ln n against L) can be derived from Equation (1) as

$$\frac{d\ln n}{dL} = -\frac{1}{G(L)\tau} - \frac{d\ln G(L)}{dL} + \frac{B(L)}{nG(L)} \qquad (3)$$

For size-independent growth, and when all nuclei are produced at zero size, the second and third terms respectively on the right hand side of Equation (3) vanish and the slope is given by the well-known expression $-1/G\tau$.

By rearranging Equation (3), the size-dependent secondary nucleation rate $B(L)$ can be expressed as

$$B(L) = nG(L)\left[\frac{d\ln n}{dL} + \frac{1}{G(L)\tau} + \frac{d\ln G(L)}{dL}\right] \qquad (4)$$

$B(L)$ can thus be obtained from a population density plot if $G(L)$ is known.

The steady state CSD from a typical MSMPR experiment is shown as a population density plot in Figure 2. The inset is an enlarged version for the size range 0-100μm. The population density plot shows slight curvature for sizes greater than about 100μm, but below this size, population density increases very much more rapidly.

Figure 3 shows the overall size-dependent growth rate, calculated by combining the surface integration rates reported previously (Garside and Jancic 1976) with the mass transfer rates applicable to the experimental crystallizer. Mass transfer rates are calculated from the correlation of Levins and Glastonbury (1972) for fluid-particle mass transfer in stirred tanks. The resulting overall growth rates become increasingly controlled by the volume diffusion step as the crystal size increases. At larger sizes, the increasing volume diffusion resistance counteracts the increasing surface integration kinetics. Above about 500 μm, the overall growth rate is almost independent of size. For small sizes, particularly below about 15 μm, overall growth is strongly size-dependent.

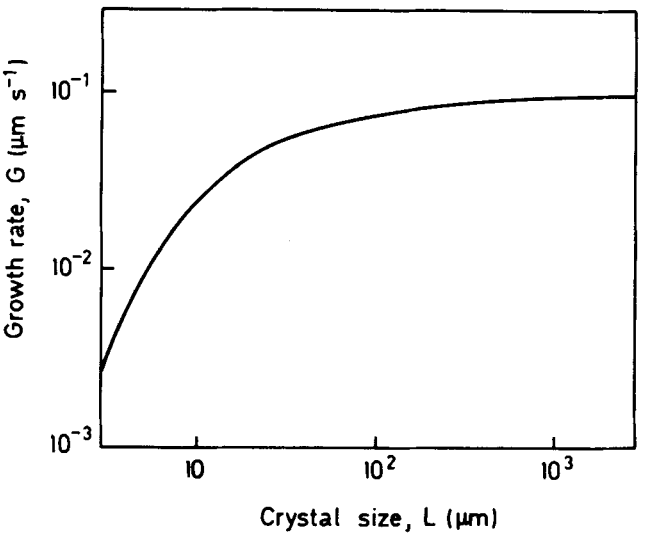

Figure 3. Estimated growth rates for the conditions used to obtain the results in Figure 2.

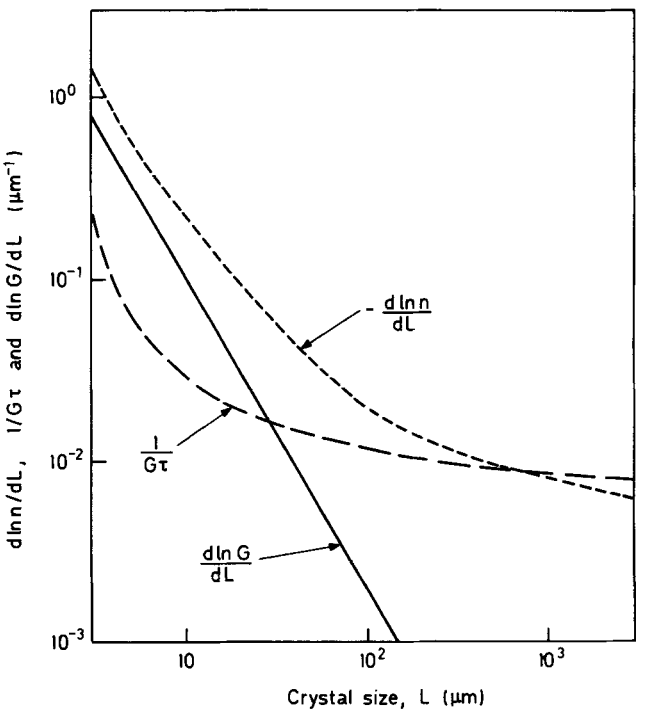

Figure 4. Values of terms appearing in the expression for nucleation rate (Equation 4), for the conditions used to obtain the results in Figures 2 and 3.

Attempts were made to estimate $B(L)$ using Equation (4) and the results shown in Figures 2 and 3. Magnitudes of the different terms on the right-hand side of Equation (4) are shown Figure 4, both $1/G(L)\tau$ and $d\ln G(L)/dL$ being obtained from the independent growth rate measurements given in Figure 3. $d\ln n/dL$ is negative for all values of L while the other two terms are positive. At small sizes the contribution from the $d\ln G(L)/dL$ term is much larger than that from $1/G(L)\tau$. At larger sizes, $d\ln G(L)/dL$ becomes negligible and $d\ln n/dL \simeq$

TABLE 2. RANGE OF EXPERIMENTAL CONDITIONS WERE PERFORMED

Variable	Crystallizer working capacity		
	1.3 litre	5 litre	30 litre
Supersaturation (kg hydrate/kg solution) $\times 10^2$	0.2-1.0	0.3-0.8	0.2-0.5
Suspension density (g/litre)	15-120	15-50	20-70
Stirrer speed (rev/min)	1,200-2,100	1,300-2,000	850-1,100
Specific power input (W/kg)	0.2-0.9	0.1-0.7	0.7-1.5
Residence time (min)	10-60	15-60	30-60

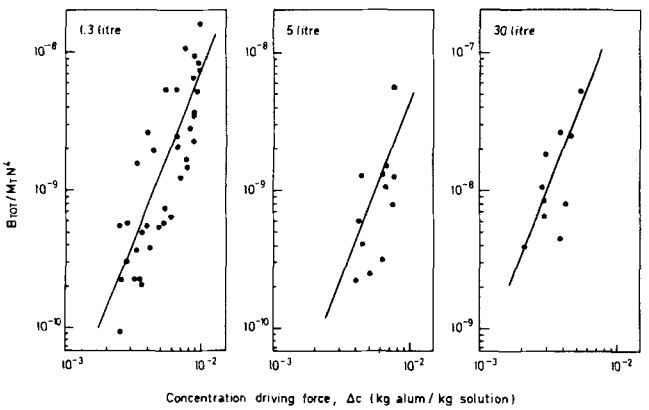

Figure 5. Modified nucleation rates for the three crystallizers; the lines represent Equation (7).

$-1/G(L)\tau$. For these larger sizes, therefore, the independent growth rate measurements give good predictions of the slope of the population density plot.

The algebraic sum of the three terms, and hence $B(L)$, is negative for sizes up to about 100 μm, indicating negative birth rates. Rather than interpret these as "death rates," it is more likely that the results are insufficiently accurate to determine $B(L)$ in this way. The calculation relies on accurate estimates of the slopes of two size-dependent functions, $n(L)$ and $G(L)$. For small sizes, the slope of both these functions is large and changes rapidly with size. At $L = 5$ μm, changes of less than 20% in the slopes would result in a positive value of $B(L)$ when using the measured value of the growth rate.

Overall nucleation rates are therefore determined from the steady-state crystal size distributions in two other ways. First, the total nucleation rate is estimated from the expression $B_{TOT} = \frac{1}{\tau}\int_0^\infty ndL$ (see Equation 2). A numerical procedure is used to evaluate this integral. All data points obtained using both sieves and Coulter Counter were used.

Secondly, the nucleation rate, based on the sieve analysis data only, B^0_{eff}, was calculated from

$$B^0_{eff} = n^0_{eff} G^0 \qquad (5)$$

The points making up the population density plot obtained using sieves (minimum sieve size = 37 μm) are fitted to a fourth order polynomial and extrapolated to $L = 0$ to obtain n^0_{eff}. The resulting "effective" nucleation rates are thus a measure of values that would be obtained using conventional sizing techniques and can be compared with the more realistic estimates represented by B_{TOT}.

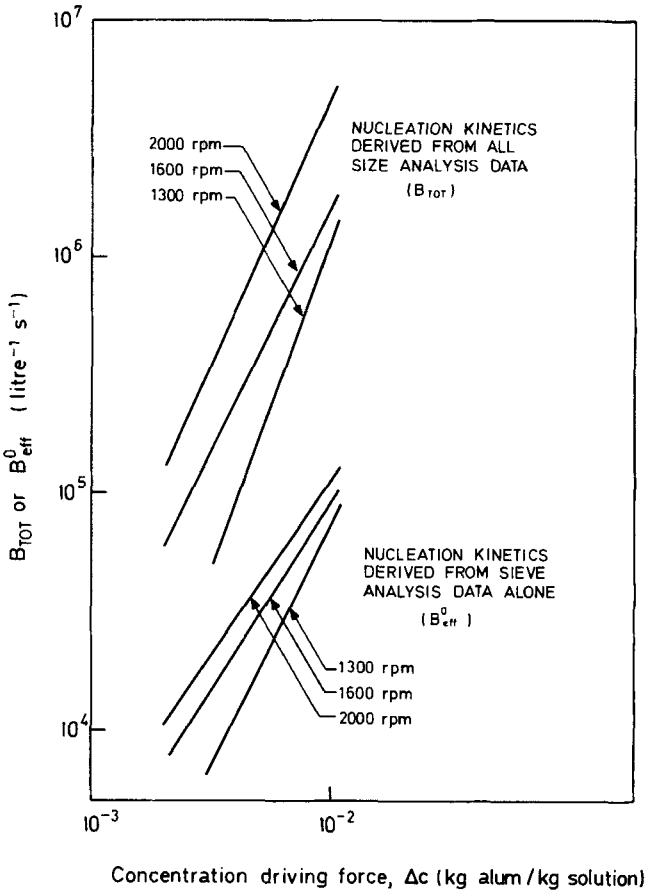

Figure 6. Comparison of B_{TOT} and B^0_{eff} for the 1.3 litre crystallizer.

NUCLEATION KINETICS

Nucleation rates in the three crystallizers are determined as a function of concentration driving force Δc, stirrer speed N, and suspension density M_T. The range of conditions covered is shown in Table 2, and a full analysis of the dependence of B_{TOT} on the individual parameters is given by Jancic (1976). The results are finally correlated by an empirical power law relation as has been used on many previous occasions

$$B_{TOT} = k_N M_T^a N^b \Delta c^m \qquad (6)$$

Compared with the results from the 1.3 litre crystallizer, fewer data points are available and the range of variables covered is significantly smaller, for both the 5 and 30 litre crystallizers. Best values of the exponents a, b, and m are therefore initially determined from the results for the 1.3 litre crystallizer. These values are consistent with the kinetics obtained in the larger crystallizers and are used to correlate the kinetics obtained in all three crystallizers. The final correlating equation is

$$B_{TOT} = k_N M_T N^{4.0} \Delta c^{2.52} \qquad (7)$$

where the values of k_N were 8.66×10^{-4}, 4.75×10^{-4} and 2.23×10^{-2} for the 1.3, 5, and 30 litre crystallizers respectively. (Units used for the variables appearing in Equation 7 are given in the Notation.) All the data points are plotted in Figure 5 in a form indicated by Equation (7).

The values of a, b, and m are typical of results obtained from other nucleation studies in continuous crystallizers. First-order dependence of nucleation rate on suspension density for example, has been found on many previous occasions and according to Ottens and de Jong (1973) indicates that the primary source of secondary nuclei is crystal/stirrer or crystal/wall collisions, rather than crystal/crystal collisions. The comparatively low-order dependence on concentration driving force is typical of secondary nucleation kinetics, while the fourth-order dependence on stirrer speed probably results from a combination of the solution hydrodynamics and the crystal/stirrer collision energy, and will be discussed in detail in the next section. Values of the constant k_N show a strong dependence on crystallizer size. This, also, results from differences in the hydrodynamics within the three crystallizers, and will be fully discussed later.

The nucleation kinetics presented in Figure 5 are derived from results obtained using experimental techniques that are often either too tedious or not available on a routine basis. For many purposes, a simple sieve analysis is the only way to determine the population density plot, and in such cases, some effective value for the nucleation rate is obtained. Figure 6 shows the correlating lines for these effective rates defined by Equation (5) as a function of Δc, obtained in the 1.3 litre crystallizer at three different stirrer speeds. For clarity, data points are not shown. Included are the lines correlating values of B_{TOT} obtained from the same runs. Effective nucleation rates, B^0_{eff}, are about an order of magnitude smaller than the total nucleation rates. Further, the order of dependence of the effective nucleation rates on both Δc and N is different from that found for B_{TOT}. Although the dependence on Δc varies somewhat with stirrer speed, this difference is not significant. The correlating equation for B^0_{eff} based on all results from the three crystallizers is

$$B^0_{eff} = k_{N(eff)}\, M_T\, N^{1.8}\, \Delta c^{2.10} \qquad (8)$$

where the values of $k_{N(eff)}$ are 82.5, 56.6, and 265 for the 1.3, 5, and 30 litre crystallizers, respectively.

Growth kinetics derived from the steady-state CSD obtained with a sieve analysis have been reported previously (Garside and Jancic 1978). The growth rates are size-dependent and were fitted to the Abegg, Stevens, and Larson (1968) growth equation:

$$G(L) = G^0\,(1 + \gamma L)^b$$

G^0 was found to be independent of hydrodynamic conditions. Results from all three crystallizers are correlated by the equation

$$G^0 = 34.3\, \Delta c^{1.33}$$

units of G^0 and Δc being defined in the Notation. The relative kinetic order i for potash alum, when kinetics are based on size analysis extending to a minimum size of about 40 μm, is thus equal to $2.10/1.33 = 1.58$.

SCALE-UP OF SECONDARY NUCLEATION KINETICS

The form of nucleation kinetics obtained in the present study suggests that nucleation is occurring by a secondary mechanism. Secondary nuclei are very easily removed from growing crystals by low energy contacts with a solid surface (Garside and Larson 1978, Garside et al. 1979), and so such a conclusion is to be expected.

Secondary nucleation rates have been correlated by Equation (7) and a reasonable fit to experimental data is obtained for each scale of operation (see Figure 5). The modified nucleation rates ($= B_{TOT}/M_T N^4$), derived from the 30 litre crystallizer, are higher than the corresponding rates for the 1.3 and 5 litre units by a factor of more than 20. Differences in flow patterns and in the efficiency of producing nuclei must, however, be taken into account before the nucleation rates from the three crystallizers can be compared on a realistic basis.

A number of authors have considered these factors (Ottens and de Jong 1972, 1973, Bennett et al. 1973, Bauer et al. 1974, Evans et al. 1974, Ramshaw 1974, Jančić 1976, Nienow 1976). Their approaches are all based on the assumption that secondary nucleation occurs as a result of contacts between crystals and other parts of the crystallizer or other crystals. Calculation of the effects of frequency and energy of such contacts are separated from the functions defining the number of secondary nuclei produced by a given contact and so, following Botsaris (1976)

$$B_{TOT} = (\dot{E}_t)\,(F_1)\,(F_2) \qquad (9)$$

where $\dot{E}_t$ is the rate of energy transfer to crystals by collisions, F_1 is the number of particles generated per unit of transferred energy and F_2 is the fraction of particles surviving to becoming nuclei. Based on the results of Clontz and McCabe (1971), all the studies assume that the number of secondary nuclei produced on the impact of a crystal is proportional to the impact energy. Little is known about the functions F_1 and F_2. They can only be determined by empirical measurements and are invariably combined and written as a simple power function of the supersaturation.

$\dot{E}_t$ is given by an equation of the form

$$\dot{E}_t = \int_0^\infty E(L)\ \omega(L)\ n(L)\ dL \qquad (10)$$

where $E(L)$ is the collision energy and $\omega(L)$ the collision frequency, both being the values appropriate to the size range L to $L + dL$. Differences in the final equations for B_{TOT} developed by various authors arise from different approaches in calculating $E(L)$ and $\omega(L)$.

Ottens and de Jong (1973) assume that the collision energy is given by

$$E(L) \propto \tfrac{1}{2} m_c v_t^2 \propto L^3 N^2 d^2 \qquad (11)$$

while the collision frequency could be written

$$\omega(L) \propto 1/t_c \propto Q_{\text{prop}}/V_c \propto C_d\, N\, d^3/V_c \qquad (12)$$

Then assuming $C_d \propto p$ (the propeller pitch) (Brothman et al., 1943)

$$\dot{E}_t \propto p\, d^5\, N^3\, \mu_3/V_c \qquad (13)$$

For flow in the fully developed turbulent region the power number N_P ($= P/\rho_s d^5 N^3$) is constant and Ottens and de Jong write the above equation as

$$\dot{E}_t \propto (p/N_P)\ \bar{\epsilon}\ \mu_3 \qquad (14)$$

where $\bar{\epsilon}$ is the specific power input. For geometrically similar crystallizers, such an approach predicts the same nucleation rate at a given specific power input (provided flow is in the fully turbulent region). For constant stirrer speed, the nucleation rate depends on S^2, where S is the linear scale of the crystallizer.

Other studies have generally been directed at evaluating more rigorous expressions for $E(L)$ and $\omega(L)$. For example, Equation (12) assumes that all crystals passing through the region of the propeller have an equal probability of collision. In practice this will not be the case, and Equation (12) is better written as

TABLE 3. COMPARISON OF SECONDARY NUCLEATION MODELS AS DEFINED BY EQUATIONS (21) AND (22)

Author	$f(G)$	b	c	j
Ottens and de Jong (1973)	pd^5/V_c	3	2	3
Evans et al. (1974)	$pd^{5.5}/V_c$	3	2.5	2.5
Jancic (1976)	$p(d^5/d_D^2)\,(V_{prop}/V_c)$	4	3	4

$$\omega(L) = \eta_p\,\omega_{exp} \tag{15}$$

where η_p is a "collision efficiency" for the propeller and ω_{exp} is the frequency of exposure to the propeller, given by Equation (12).

Evans et al. (1974) use a numerical simulation describing the trajectory of a particle past the propeller to estimate both η_p (which they termed "efficiency of collection") and the collision velocity. For collisions between crystals and propeller arising from the bulk flow, the resulting equation is of the form

$$\dot{E}_t \propto p\,d^{5.5}\,N^3\,\mu_{2.5}/V_c \propto (p/N_P)\,\bar{\epsilon}\,d^{0.5}\,\mu_{2.5} \tag{16}$$

Bauer et al. (1974), Jancic (1976) and Nienow (1976) suggest that a "target efficiency" could be used to represent η_p. By analogy with the general problem of particle collisions with a moving object (e.g. Bosenquet 1950, Perry and Chilton 1973), the target efficiency would be expected to be a function of a dimensionless 'separation number' N_{sep}, which for the present case can be defined by

$$N_{sep} = v_t\,u_t/d\,g \tag{17}$$

The crystal terminal velocity is given by

$$u_t = \left[\frac{4gL\,(\rho_c - \rho_s)}{3\rho_s\,c_D}\right]^{1/2}$$

Crystal size distributions grown in continuous crystallizers comprise a wide range of sizes so a unique definition of the corresponding drag coefficients in terms of Reynolds numbers is difficult. Jancic (1976) assumes that crystals in the Stokes' law region ($Re < 2$) do not collide with the impeller blades and that there are very few crystals in the Newton's law region ($Re > 500$). The drag coefficient may then be represented by the empirical equation for spheres in the intermediate region, $c_D = 18.5/N_{Re}^{0.6}$ For potash alum crystals growing in slightly supersaturated solution at 30°C the intermediate region corresponds to the size range between about 150 and 2,500 μm. In this case, the terminal velocity for a given crystallizing system (i.e. constant physical properties) is represented as $u_{t\alpha}\,L^{1.14}$ or to an approximately linear dependence of terminal velocity on crystal size. Thus, for a given system Jancic writes Equation (17) as

$$N_{sep} \propto \frac{(Nd)\,L}{d} \propto NL \tag{18}$$

He also suggests that two other parameters will affect the collision efficiency in the DTB configuration used in the present study. First, the ratio of projected propeller blade area in the plane perpendicular to the axis of rotation, A_B, to the cross-sectional area of the draft-tube $\pi d_D^2/4$, will affect the probability of whether a particle will traverse the propeller area. Second, the crystal residence time in the propeller area will affect the probability of collision, and for a given circulation velocity, will be a function of the width of the propeller blades, H. The collision efficiency is thus written as

$$\eta_p \propto NL\,A_B\,H/d_D^2 \propto NL\,V_{prop}/d_D^2 \tag{19}$$

and so

$$\dot{E}_t \propto p(d^5/d_D^2)\,(V_{prop}/V_c)N^4\mu_4 \tag{20}$$

All the above developments give rise to nucleation rate equations having the general form

$$B_{TOT} = K_N f(G)\,N^b\,\mu_j\,\Delta c^m \tag{21}$$

where $f(G)$ is a function of crystallizer geometry and size. For geometrically similar vessels, the size of which is characterized by a length scale S, Equation (21) can be written

$$B_{TOT} \propto S^c\,N^b\,\mu_j\,\Delta c^m \tag{22}$$

Values of $f(G)$, b, c and j are summarized in Table 3 for the equations of Ottens and de Jong (1973), Evans et al. (1974), and Jancic (1976).

The experimental nucleation rates shown in Figure 5 and represented by Equation (7) are compared with these expressions. In all cases, j was taken as 3, since in practice the third moment is comparatively simple to measure and is directly related to process design parameters. Thus $\mu_j = M_T$, the suspension density. On the basis of Equation (21), B_{TOT}/N^bM_T was correlated with Δc to determine $K_N f(G)$ and m. The best value of m was 2.52 when $b = 4$ [as given in Equation (7)] and 2.43 when $b = 3$. The ratio of $K_Nf(G)$ for the 5 or 30 litre crystallizer to that for the 1.3 litre vessel should then equal the corresponding ratios of $f(G)$ determined from the vessel geometry. The results of these calculations are shown in Table 4.

All three approaches are reasonably successful in predicting the differences in nucleation rates obtained in the three crystallizers. Starting with the kinetics in the 1.3 litre vessel, the equation of Jancic is most reliable in predicting the nucleation rate on the 5 litre scale, while that of Ottens gives excellent agreement with the rate found in the 30 litre crystallizer. Considering the scatter of the experimental data illustrated in Figure 5, it is not possible to distinguish between the relative merits of the three approaches. It is, however, noteworthy that the secondary nucleation kinetics represented by Equation (7) were found to follow a fourth-order dependence on stirred speed, as suggested by the development of Jancic.

TABLE 4. RATIOS OF $f(G)/f(G)_{1.3\ litre}$ AS PREDICTED BY DIFFERENT AUTHORS, COMPARING GEOMETRIC AND HYDRODYNAMIC CONSIDERATIONS WITH EXPERIMENTAL VALUES CALCULATED FROM MEASURED NUCLEATION KINETICS

Crystallizer capacity (litre)	Ottens and de Jong (1973)		Evans et al. (1974)		Jancic (1976)	
	Geometry	Kinetics	Geometry	Kinetics	Geometry	Kinetics
5	1.96	0.50	2.51	0.50	1.02	0.55
30	14.0	14.2	24.3	14.2	38.3	25.8

DISCUSSION

One of the objectives of this study is to determine the size-dependent secondary nucleation rate in a conventional MSMPR crystallizer from independent measurements of the size-dependent crystal growth rate and the population density. This part of the study is not successful. A number of different factors are responsible for this.

Firstly, the shape of the population density plot (Figure 2) suggests that many secondary nuclei are produced at sizes smaller than the minimum size down to which measurements were made, i.e., below about 5 μm. This has been confirmed by direct observation and measurement (Garside and Larson 1978, Garside et al. 1979). Limitations in the experimental technique associated with the Coulter Counter prevents measurements being made in smaller size ranges, but even if the experimental difficulties had been overcome and measurements at smaller sizes achieved, difficulties in interpretation would still remain.

Randolph and his co-workers (Randolph and Cise 1972, Youngquist and Randolph 1972) used a similar Coulter Counter and obtained data points down to about 2 μm when measuring CSDs resulting from secondary nucleation in a "mini-nucleator." Their population density plots are very similar in shape to those reported here, but they encountered similar problems in calculating and interpreting nucleation rates. As Youngquist and Randolph (1972) point out, their calculation procedure inevitably introduces a degree of arbitrariness into the definition of total nucleation rate, since data points are not available down to the smallest size at which secondary nuclei are produced. Extrapolation through small size ranges still has to be employed, and it is in the very small size ranges that growth and nucleation rates appear to be most strongly dependent on crystal size.

Second, the accuracy required in determining $n(L)$ and $G(L)$ at very small sizes for the subsequent determination of $B(L)$ was not achieved (this point has been discussed earlier).

For potash alum, the sharp increase in population density at small sizes results from a combination of size-dependent growth rates and a size-dependent secondary nucleation mechanism. Two limiting assumptions made in some previous studies, 1) that growth rates of very small crystals are zero or 2) that all nuclei are produced at zero size, are both invalid for potash alum. Growth rates of crystals in the larger size-ranges measured in independent experiments are in good agreement with rates deduced from the crystal size distribution, as can be seen from Figure 4 and from other results (Garside and Jancic 1978). Prediction of growth kinetics for a wide range of hydrodynamic conditions from measurements under quite different conditions can be made. Use of a simple series-resistance model of crystal growth with conventional mass transfer correlations describing the bulk diffusion resistance appears a reasonably reliable technique.

Nucleation kinetics are very much more difficult to scale-up. Nevertheless, the models for secondary nucleation derived from Equation (10) and compared here are reasonably successful. The success of such equations can be assessed by using the nucleation kinetics in the 1.3 litre crystallizer to predict the rates in the 5 and 30 litre vessels. Figure 7 shows these predictions made on the basis of Jancic's equation (Equation 20), together with the experimental rates from the two larger vessels. While the predicted values are somewhat higher than the measured points, the difference does not exceed a factor of 2. The

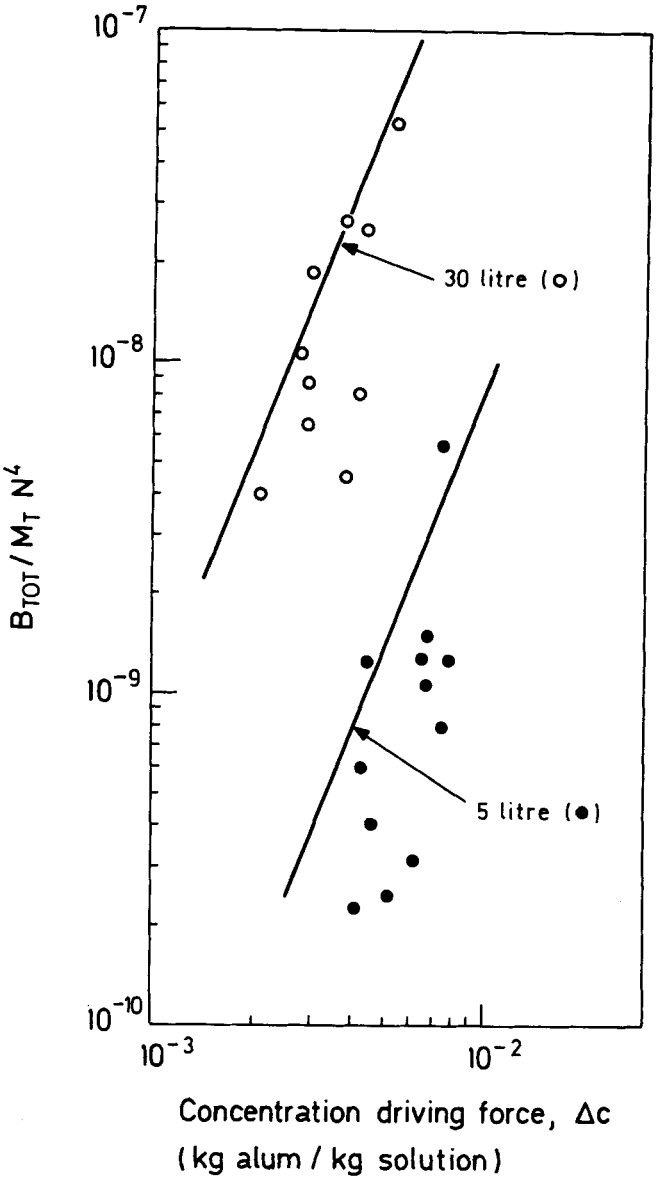

Figure 7. Prediction of nucleation rates in the 5 and 30 litre crystallizers from measurements in the 1.3 litre crystallizer, using Equation (20) (solid lines). Points show experimental nucleation rates.

greatly enhanced nucleation rates in the 30 litre vessel are in line with those predicted by the equation.

Nucleation models used here assume that all nuclei are generated by crystal/propeller collisions. The success of such models, therefore, supports the view that such collisions are the dominant mode of nuclei production for the potash alum/water system. Maximum suspension density used in this study is about 120 g crystals/litre solution, and this only in the 1.3 litre crystallizer (see Table 2). Many industrial crystallizers operate with suspension densities two or more times higher than this. Under such conditions, crystal/crystal collisions may become a significant source of nuclei.

Nucleation kinetics derived using the Coulter Counter [Equation (7)] and sieves [Equation (8)] result not only in very different absolute nucleation rates, but also in a different dependence of nucleation rate on both stirrer speed and concentration driving force. The relation between these two nucleation rates can be explored using the simple model shown in Figure 8. This represents an experimental population density plot obtained in an MSMPR crystallizer under conditions of size-dependent growth.

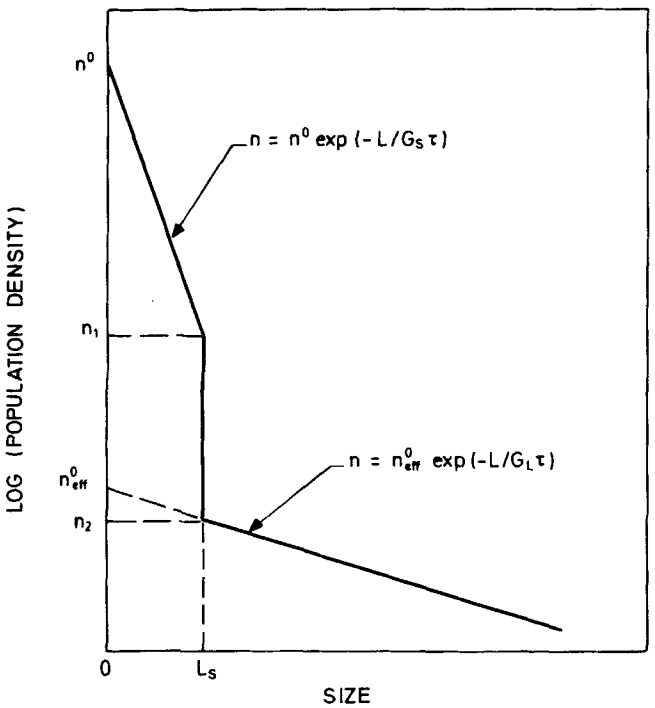

Figure 8. Simplified model for growth rates of small crystals.

The CSD in the small size range ($0 \leq L \leq L_S$) is approximated by a straight line, with a slope corresponding to some effective growth rate of small crystals G_S. Similarly, the CSD in the large size range ($L \geq L_S$) is also represented by a straight line, with the slope corresponding to an effective growth rate of large crystals, G_L. The discontinuity at L_S occurs since at this point the number flux must be continuous and so

$$n_1 G_S = n_2 G_L, \quad \text{at} \quad L = L_S \tag{23}$$

Hence, $n_1 > n_2$ if $G_L > G_S$. The resulting population density plot is an approximation to that obtained in the present work with $L_S \simeq 30$ μm.

For the size range $0 \leq L \leq L_S$,

$$n = n^0 \exp\,(-L/G_S\tau)$$

while for $L \geq L_S$

$$n = n^0{}_{\text{eff}} \exp\,(-L/G_L\tau)$$

Substituting into Equation (23) gives

$$G_S n^0 \exp\,(-L_S/G_S\tau) = G_L n^0{}_{\text{eff}} \exp\,(-L_S/G_L\tau)$$

or

$$\frac{n^0{}_{\text{eff}}}{n^0} = \frac{G_S}{G_L} \exp\left[\frac{L_S}{\tau}\left(\frac{1}{G_L} - \frac{1}{G_S}\right)\right] \tag{24}$$

This description is similar to that for an MSMPR crystallizer with fines destruction (Randolph and Larson 1971, Larson and Garside 1973). In the present case, however, it is the difference in growth rate for small and large crystals rather than difference in residence time that results in "wash-out" or "destruction" of fines.

From Equation (24), provided $G_S < G_L$, then $n^0{}_{\text{eff}} < n^0$, i.e., the effective nuclei population density is less than the "true" value, n^0.

Writing $B^0 = n^0\, G_S$ (so assuming all nuclei are produced at $L = 0$) and $B^0{}_{\text{eff}} = n^0{}_{\text{eff}}\, G_L$, where B^0 can be thought of as the "true" nucleation rate and $B^0{}_{\text{eff}}$ as the effective rate, Equation (24) can be rewritten

$$\frac{B^0{}_{\text{eff}}}{B^0} = \exp\left[\frac{L_S}{\tau}\left(\frac{1}{G_L} - \frac{1}{G_S}\right)\right] \tag{25}$$

where $B^0{}_{\text{eff}}/B^0$ is the fraction of nuclei which are retained in the crystallizer for a sufficient length of time to populate the larger size ranges. Letting $\tau_S = L_S/G_S$, the time for nuclei to grow to size L_S, and $\tau_L = L_S/G_L$ which represents the time for the nuclei to grow to size L_S if they grew at the same rate as the larger crystals, Equation (25) can be expressed as

$$\frac{B^0{}_{\text{eff}}}{B^0} = \exp\left(\frac{\tau_L - \tau_S}{\tau}\right) \tag{26}$$

Finally, if $G_S << G_L$, then $\tau_L << \tau_S$ and Equations (25) and (26) can be simplified to give

$$\frac{B^0{}_{\text{eff}}}{B^0} \simeq \exp\left(-\frac{L_S}{G_S\tau}\right) = \exp\left(-\frac{\tau_S}{\tau}\right) \tag{27}$$

Equation (27) indicates that the value of $B^0{}_{\text{eff}}/B^0$ is a function of the ratio τ_S/τ. The effective nucleation rate, therefore, depends on the growth rate of the small crystals and the value of L_S and, to a lesser extent, on the growth rate of large crystals [see Equation (25)]. It depends also on the crystallizer residence time. If the residence time is sufficiently long for significant numbers of small crystals to grow to larger sizes, then $B^0{}_{\text{eff}}$ will approach B^0. For very short residence times, on the other hand, the vast majority of nuclei will be washed out of the crystallizer before they have chance to grow and populate the larger sizes and so $B^0{}_{\text{eff}}$ will be very much less than B^0.

The dependence of $B^0{}_{\text{eff}}$ on concentration driving force and stirrer speed can be deduced from Equation (25). The nucleation rate is given by an equation of the form shown in Equation (6):

$$B^0 \propto N^b\, \Delta c^m \tag{28}$$

while the growth rates of small and large crystals can be written

$$G_S \propto \Delta c^e \tag{29}$$

and

$$G_L \propto N^c\, \Delta c^f \tag{30}$$

In general, growth rates of small crystals will be surface integration controlled (Garside et al. 1976, Garside and Jancic 1976), and so will be independent of stirrer speed. The growth rate of larger crystals may be affected by stirrer speed if diffusion of solute to the crystal surface offers significant resistance to the growth process. In general, $0 \leq c \leq 0.5$.

Combining Equations (28)-(30) with Equation (25) gives

$$B^0{}_{\text{eff}} \propto N^b\, \Delta c^m \exp\left[\frac{L_S}{\tau}\left(\frac{\alpha}{N^c \Delta c^f} - \frac{\beta}{\Delta c^e}\right)\right] \tag{31}$$

where α and β are constants at a given Δc and N. $B^0{}_{\text{eff}}$ depends on Δc and N in a complicated manner since these two variables appear in both the pre-exponential and the exponential terms. Further $B^0{}_{\text{eff}}$ is a function of residence time, which itself affects the steady-state value of Δc in the crystallizer.

The above arguments emphasize the inherent arbitrariness and empiricism involved in correlations for $B^0{}_{\text{eff}}$. The similarity of the exponents of Δc and the difference in the exponents of N shown in Equations (7) and (8) are probably coincidental, and little or no information concerning the mechanism of nucleation can be obtained from measurements of $B^0{}_{\text{eff}}$. This is not to say that such measurements cannot be used for design or crystallizer evaluation purposes. Indeed, there is evidence that they are extremely valuable. The empirical nature and sub-

sequent limitations of such measurements must, however, be recognized.

NOTATION

a = exponent of magma density, Equation (6)
A_B = projected propeller blade area
b = exponent of stirred speed, Equations (6) and (21)
B_{TOT} = total nucleation rate, Equation (2), s litre
B_L = birth function
$B(L)_{TOT}$ = total secondary nucleation rate
B^0_{eff} = nucleation rate determined using sieves, s litre
c = exponent of length scale, Equation (22)
c_D = drag coefficient
Δc = concentration driving force, g alum/g solution
C_d = propeller discharge coefficient
d_D = draft-tube diameter
d = stirrer diameter
$\dot{E}_t$ = rate of energy transfer to crystals
$E(L)$ = collision energy
$f(G)$ = geometric parameter, Equation (21)
g = acceleration due to gravity
$G(L)$ = size-dependent growth rate
G^0 = growth rate at $L = 0$, μm/s
G_L = growth rate of large crystals ($L > L_S$)
G_S = growth rate of small crystals ($0 < L < L_S$)
H = width of impeller blades
k_N, $k_{N(\text{eff})}$, K_N = nucleation constants as defined in Equations (6), (8), and (21), respectively
L = characteristic crystal size
L_S = crystal size below which growth rate is G_S
m = exponent of Δc, Equation (6)
m_c = mass of a single crystal
M_T = suspension density, g/litre
n = population density
n^0 = population density at $L = 0$
n^0_{eff} = population density at $L = 0$, determined using sieves
N = stirrer speed, rev/min
N_P = power number
N_{Re} = particle Reynolds number
N_{sep} = separation number
p = propeller pitch
P = power input
Q_{prop} = pumping capacity of propeller
S = length scale
t_c = circulation time
u_t = crystal terminal velocity
v_t = propeller tip velocity
V_c = crystallizer volume
V_{prop} = volume swept by propeller

Greek Letters

α, β = constants in Equation (31)
$\bar{\epsilon}$ = specific power input
μ_j = j^{th} moment of crystal size distribution
ρ_c = crystal density
ρ_s = solution density
η_p = collision efficiency in propeller area
τ = crystallizer residence time
τ_L, τ_S = growth times for small crystals, see Equation (26)
$\omega(L)$ = collision frequency between crystal and propeller
ω_{exp} = exposure frequency of crystal to propeller area

LITERATURE CITED

Abegg, C. F., J. D. Stevens, M. A. Larson, "Crystal Size Distribution in Continuous Crystallizers when Growth Rate is Size Dependent," *AIChE J.*, **14**, 118 (1968).

Bauer, L. G., R. W. Rousseau, W. L. McCabe, "Influence of Crystal Size on the Rate of Contact Nucleation in Stirred-Tank Crystallizers," *AIChE J.*, **20**, 653 (1974).

Bennett, R. C., H. Fiedelman, A. D. Randolph, "Crystallizer Influenced Nucleation," *Chem. Eng. Prog.*, **69** (7), 86 (1973).

Bosanquet, C. H., "Impingement of Particles on Obstacles in a Stream," *Trans. Inst. Chem. Eng.*, **28**, 136 (1950).

Botsaris, G. D., "Secondary Nucleation—A Review," in *Industrial Crystallization*, p. 3, Plenum Press, New York (1976).

British Standards Specification 410:1969, "Test Sieves," British Standards Inst., London (1969).

Brothman, A., A. P. Weber, E. Z. Barish, "New Approach to Continuous Reactor Design," *Chem. Met. Eng.*, **50**, 107 (1943).

Bujac, P. D. B., "Attrition and Secondary Nucleation in Agitated Crystal Slurries," in *Industrial Crystallization*, p. 25, Plenum Press, New York (1976).

Clontz, N. A., W. L. McCabe, "Contact Nucleation of Magnesium Sulphate Heptahydrate," *Chem. Eng. Prog.*, Symp. Ser. **67**, (110), 6 (1971).

Evans, T. W., A. F. Sarofim, G. Margolis, "Models of Secondary Nucleation Attributable to Crystal-Crystallizer and Crystal-Crystal Collisions," *AIChE J.*, **20**, 959 (1974).

Garside, J., "The Growth of Small Crystals," paper presented at 7th Symposium on Industrial Crystallization, Warsaw (September, 1978).

Garside, J., S. J. Jančić, "Growth and Dissolution of Potash Alum Crystals in the Subsieve Size Range," *AIChE J.*, **22**, 887 (1976).

Garside, J., S. J. Jančić, "Prediction and Measurement of Crystal Size Distributions for Size-Dependent Growth," *Chem. Eng. Sci.*, **33**, 1623 (1978).

Garside, J., M. A. Larson, "Direct Observation of Secondary Nuclei Production," *J. Cryst. Growth*, **43**, 694 (1978).

Garside, J., V. R. Phillips, M. B. Shah, "On Size-Dependent Crystal Growth," *Ind. Eng. Chem., Fundam.*, **15**, 230 (1976).

Garside, J., I. T. Rusli, M. A. Larson, "Origin and Size Distribution of Secondary Nuclei," *AIChE J.*, **25**, 57 (1979).

Jančić, S. J., J. Garside, "On the Determination of Crystallization Kinetics from Crystal Size Distribution Data," *Chem. Eng. Sci.*, **30**, 1299 (1975).

Jančić, S. J., "Crystallization Kinetics and Crystal Size Distributions in Mixed Suspension Mixed Product Removal Crystallizers," Ph.D. thesis, University of London, England (1976).

Jones, A. G., J. W. Mullin, "Crystallization Kinetics of Potassium Sulphate in a Draft-Tube Agitated Vessel," *Trans. Inst. Chem. Eng.*, **51**, 302 (1973).

Larson, M. A., J. Garside, "Crystallizer Design Techniques Using the Population Balance," *The Chemical Engineer*, No. 274, 318 (1973).

Larson, M. A., L. L. Bendig, "Nuclei Generation from Repetitive Contacting," *Chem. Eng. Prog.*, Symp. Ser. **72** (153), 21 (1976).

Levins, D. M., J. R. Glastonbury, "Particle-Liquid Hydrodynamics and Mass Transfer in a Stirred Vessel," *Trans. Inst. Chem. Eng.*, **50**, 132 (1972).

Manjaly, J., "The Effect of Power Input and Impeller Material of Construction on Crystallization Kinetics in a Continuous Crystallizer," M. Phil. Thesis, University of London, England (1978).

Mullin, J. W., J. Garside, "The Crystallization of Aluminium Potassium Sulphate: A Study in the Assessment of Crystallizer Design Data," *Trans. Inst. Chem. Eng.*, **45**, T291 (1967).

Nienow, A. W., "The Effect of Agitation and Scale-Up on Crystal Growth Rates and on Secondary Nucleation," *Trans. Inst. Chem. Eng.*, **54**, 205 (1976).

Ottens, E. P. K., A. H. Janse, E. J. de Jong, "Secondary Nucleation in a Stirred Vessel Cooling Crystallizer," *J. Cryst. Growth*, **13/14**, 500 (1972).

Ottens, E. P. K., E. J. de Jong, "A Model for Secondary Nucleation in a Stirred Vessel Cooling Crystallizer," *Ind. Eng. Chem., Fundam.*, **12**, 179 (1973).

Perry, R. H., C. H. Chilton, *Chemical Engineers Handbook*, 5th ed., p. 20-80, McGraw-Hill, New York (1973).

Ramshaw, C., "Secondary Nucleation in Mechanically Agitated Crystallizers: Crystal Motion in the Impeller Region," *The Chemical Engineer*, No. 287/8, 446 (1974).
Randolph, A. D., M. A. Larson, *Theory of Particulate Processes*, Academic Press, New York (1971).
Randolph, A. D., M. D. Cise, "Nucleation Kinetics of the Potassium Sulphate-Water System," *AIChE J.*, 18, 798 (1972).
Rusli, I. T., "Origin, Size Distribution and Growth of Small Crystals in Contact Nucleation," M.S. thesis, Chemical Engineering Department, Iowa State University (1978).
van't Land, C. M., B. G. Wienk, "Control of Particle Size in Industrial NaCl Crystallization," in *Industrial Crystallization*, p. 51, Plenum Press, New York (1976).
Youngquist, G. R., A. D. Randolph, "Secondary Nucleation in a Class II System: Ammonium Sulphate-Water," *AIChE J.*, 18, 421 (1972).

Manuscript received August 3, 1978; revision received May 4, and accepted May 7, 1979.

Heat Transfer with Stratified Gas-Liquid Flow

E. JAMES DAVIS
NICHOLAS P. CHEREMISINOFF
and
CHRISTOPHER J. GUZY

Department of Chemical Engineering
Clarkson College of Technology
Potsdam, New York 13676

This article presents a method for predicting local Nusselt numbers for heat transfer to a stratified gas-liquid flow for turbulent liquid/turbulent gas conditions. A mathematical model based on the analogy between momentum transfer and heat transfer is developed and tested, using heat transfer and fluid mechanics data taken for air/water flow in a 63.5 mm I.D. tube. The fluid mechanics parameters required for the prediction of the heat transfer characteristics are obtained in the manner outlined elsewhere. Liquid phase Nusselt numbers predicted by the analogy are shown to be in agreement with experimental results for large and small amplitude wavy interfacial conditions. The circumferential average gas phase Nusselt numbers are in rough agreement with the Dittus-Boelter equation for single phase flow based on flow through a conduit of irregular shape. There is a tendency for the average gas phase Nusselt numbers to scatter about predicted values because of the effects of splashing and droplet deposition on the tube wall in the vicinity of the gas-liquid interface.

SCOPE

Two-phase gas-liquid flow with heat transfer occurs in a variety of process equipment, including feed preheaters for gas-liquid reactors, cooler/condensers, reboilers, evaporators and distillation equipment. Horizontal stratified flows occurring in heat exchange equipment involve heat transfer to both phases, and the prediction of the heat transfer characteristics is complicated by the existence of interfacial waves and droplet formation at higher gas and liquid flow rates. Depending on the flow rates, small amplitude capillary waves or large amplitude roll waves occur, and when the gas flow rate is sufficiently high, significant droplet entrainment occurs—to further complicate the heat transfer process.

In this article, we analyze and support by experimental data, the transfer of heat to a turbulent/turbulent stratified flow in a horizontal pipe. Fluid flow characteristics of stratified gas-liquid flows are now reasonably predictable due, to the studies of Yu and Sparrow (1967) on laminar/laminar flows, of Etchells (1970), Govier and Aziz (1972), Agarwal et al. (1973) and Russell et al. (1974) on laminar liquid/turbulent gas flows and of Cheremisinoff and Davis (1979) in a companion paper on turbulent/turbulent flows. But considerably less work of a fundamental nature has been done on the heat transfer characteristics of such flows. Rosson and Myers (1965) and Davis (1975) had considerable success in applying the von Karman analogy to gas-liquid flow heat transfer, and we extend these concepts and test the analysis with new data for air/water flow.

CONCLUSIONS AND SIGNIFICANCE

An analogy between momentum transfer and heat transfer can be applied to predict the heat transfer characteristics of the liquid layer of a stratified gas-liquid flow, even when appreciable wave action occurs at the gas-liquid interface. Using wall shear stresses predicted by the method outlined in a companion paper and using the geometric model of that paper, we predict liquid phase Nusselt numbers within 20% of measured values over a fairly wide range of flow rates and interfacial conditions. Even when some droplet entrainment occurs, our analysis agrees with experiments, but such agreement cannot be expected to hold at high gas flow rates, for which an appreciable fraction of the liquid is entrained.

Current address for Davis and Guzy: Department of Chemical and Nuclear Engineering, University of New Mexico, Albuquerque, NM 87131.

0065-8812-79-3055-0958-$01.05.